Competing Pairing Symmetries in a Generalized Two-Orbital Model for the Pnictide Superconductors

Andrew Nicholson,[1,2] Weihao Ge,[1,2] Xiaotian Zhang,[1,2] José Riera,[3] Maria Daghofer,[4] Andrzej M. Oleś,[5,6] George B. Martins,[7] Adriana Moreo,[1,2] and Elbio Dagotto[1,2]

[1]*Department of Physics and Astronomy, The University of Tennessee, Knoxville, Tennessee 37996, USA*
[2]*Materials Science and Technology Division, Oak Ridge National Laboratory, Oak Ridge, Tennessee 32831, USA*
[3]*Instituto de Física Rosario, Universidad Nacional de Rosario, 2000-Rosario, Argentina*
[4]*IFW Dresden, P.O. Box 27 01 16, D-01171 Dresden, Germany*
[5]*Max-Planck-Institut fur Festkorperforschung, Heisenbergstrasse 1, 70569 Stuttgart, Germany*
[6]*M. Smoluchowski Institute of Physics, Jagellonian University, Reymonta 4, 30-059 Kraków, Poland*
[7]*Department of Physics, Oakland University, Rochester, Michigan 48309, USA*

(Received 5 October 2010; published 24 May 2011)

We introduce and study an extended "*t*-*U*-*J*" two-orbital model for the pnictides that includes Heisenberg terms deduced from the strong coupling expansion. Including these J terms explicitly allows us to enhance the strength of the $(\pi, 0)$-$(0, \pi)$ spin order which favors the presence of tightly bound pairing states even in the small clusters that are here exactly diagonalized. The A_{1g} and B_{2g} pairing symmetries are found to compete in the realistic spin-ordered and metallic regime. The dynamical pairing susceptibility additionally unveils low-lying B_{1g} states, suggesting that small changes in parameters may render any of the three channels stable.

DOI: 10.1103/PhysRevLett.106.217002 PACS numbers: 74.20.Rp, 71.10.Fd, 74.20.Mn, 74.70.Xa

Introduction.—One of the main puzzles in iron-based superconductors [1] arises from the conflicting experimental results on the presence of nodes in the superconducting state. Surface-sensitive angle-resolved photoemission (ARPES) studies [2] indicate that full nearly momentum-independent gaps open on all Fermi surface (FS) pockets. However, some bulk experiments give results compatible with nodal superconductivity [3]. On the theory side, calculations where many different pairing states are allowed to compete, as opposed to studying a few isolated states, are difficult for multiorbital Hubbard models. Within magnetic mechanisms for superconductivity, two approaches have addressed this issue: (i) random phase approximation (RPA) studies suggested that several pairing channels are in competition [4], in agreement with (ii) two-orbital model Lanczos studies [5,6] based on the quantum numbers of the state with two more electrons than half filling. However, RPA relies on a particular subset of diagrams, while studying the quantum numbers of clusters did work before for the cuprates [7], but finding true Cooper pair formation is difficult.

In this Letter, a simple generalization of Hubbard models for pnictides is presented that increases the strength of the $(\pi, 0)$-$(0, \pi)$ spin order in the undoped limit, creating tightly bound states upon electronic doping that can be studied with Lanczos methods on the small clusters currently accessible with state-of-the-art computers. These extra terms can be justified by noting that the undoped state, which combines itinerant electrons with a robust Néel temperature and a lattice distortion [8], is itself rather exotic and suggests a more stable magnetic order than a description based exclusively on on-site Coulomb repulsion would support. The *t*-*J* model for cuprates [9] provides further guidance: here J, when considered as independent of t, can be increased to sufficiently large values that d-wave pairing tendencies are amplified and tightly bound states are formed, while in the Hubbard model the d-wave pairing signal is weak [9]. In pnictides, the strong coupling t-J_1-J_2 model has been studied before [10]. In the alternative "*t*-*U*-*J*" route [11] to be followed here, Heisenberg "J" terms will be added to the original Hubbard model to enhance spin order and pairing tendencies, but without projecting out doubly occupied sites and charge fluctuations.

Model and method.—The two-orbital model [5,6,12] based on the d_{xz} (x) and d_{yz} (y) Fe orbitals is studied here. Keeping only these two orbitals is reasonable since x and y provide the largest contribution to the pnictides' band structure FS [13]. In addition, the studies described below are computationally demanding and they simply *cannot* be carried out with more orbitals. Thus, a balance must be reached between the more ideal five-orbital models and the feasibility of the actual calculations. The model includes a hopping term with amplitudes that fit band calculations [12] (energy scale $|t_1|$), a Hubbard term with on-site intraorbital repulsion U, a Hund coupling J_H, an interorbital repulsion fixed as $U' = U - 2J_H$, and a pair-hopping term with coupling $J' = J_H$ [14]. The model was used in several previous studies [6]. The novelty is the extra Heisenberg terms that will be added, with associated exchange couplings for nearest-neighbor (NN) and next-nearest-neighbor (NNN), J_{NN} and J_{NNN}, as discussed below.

The two-orbital Hamiltonian is exactly investigated using the Lanczos algorithm (including dynamical information) on a small tilted $\sqrt{8} \times \sqrt{8}$ cluster [5,6,9]. This requires substantial computational resources: to determine the undoped-limit ground state of the 8-sites cluster even exploiting the Hamiltonian symmetries still requires a basis with ~2–20 M states (equivalent to a 16-sites cluster one-band Hubbard model) depending on the subspace explored. Lanczos runs had to be performed for all allowed momenta $\mathbf{k}$, quantum numbers under rotations and reflections (i.e., irreducible representations A_{1g}, A_{2g}, B_{1g}, B_{2g}, and E of the D_{4h} group [6,15]), and z-axis total spin projections. In addition, binding energies require calculations for a number of electrons N equal to 16, 17, and 18, varying U, J_H, $J_{\rm NN}$, and $J_{\rm NNN}$ in a fine grid. The full effort amounted to ~8000 diagonalizations of the cluster, supplemented by dynamical calculations, using a Penguin 128GB Altus 3600 computer.

Results for the original two-orbital model.—The relative symmetry between the undoped ($N = 16$) ground state (GS) and the $N = 18$ GS has been studied varying $U/|t_1|$ and J_H/U. The results at $J_{\rm NN} = J_{\rm NNN} = 0$ are shown in Fig. 1(a). The undoped GS has momentum $\mathbf{k} = (0, 0)$ and it transforms according to the A_{1g} representation of the D_{4h} group, for all the investigated values of J_H and U. The $N = 18$ GS also has $\mathbf{k} = (0, 0)$, but its irreducible representation varies in different regions of the phase diagram. In agreement with previous results [6], the $N = 18$ GS is a spin triplet for $U \leq 6|t_1|$ [16] and a broad range of J_H/U. A spin-singlet state with symmetry B_{2g} dominates the small J_H/U (roughly ≤ 0.15) region for the studied values of $U/|t_1|$. This B_{2g} state arises from the orbital portion of the pairing operator since the two extra electrons added to the undoped GS are located in different orbitals [6]. At $U \geq 7|t_1|$ and intermediate to large J_H/U regimes, the singlet-state symmetry becomes A_{1g}. The binding energy

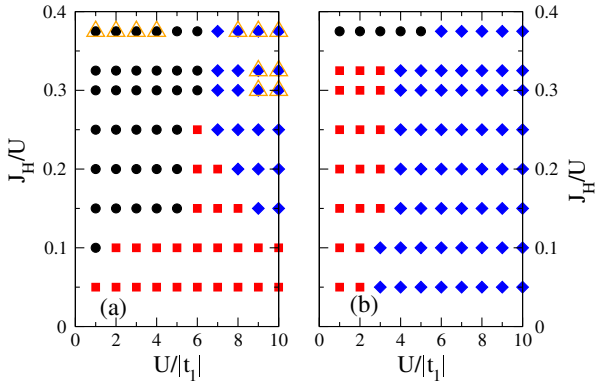

FIG. 1 (color online). Relative symmetry between the $N = 16$ (undoped) and $N = 18$ GSs, varying U and J_H/U. Circles denote triplet states, squares B_{2g}-symmetric singlets, and diamonds A_{1g}-symmetric singlets. (a) Results for couplings $J_{\rm NN} = J_{\rm NNN} = 0$. Open triangles indicate binding. (b) Results for the lowest value of $(J_{\rm NN}, J_{\rm NNN})$ where binding appears.

$E_B = E(18) + E(16) - 2E(17)$, where $E(N)$ is the GS energy of N electrons, was also studied. Binding, i.e., $E_B < 0$, is observed but only at large U's where the undoped GS is an insulator.

Binding stabilization.—As discussed in the introduction, here the spin background with wave vectors $(\pi, 0)$-$(0, \pi)$ will be magnified via the addition of extra Heisenberg terms with the expectation that carrier attraction will become stronger, leading to $E_B < 0$ pairing. To find the precise form of the Heisenberg terms, a strong coupling (large U and J_H) expansion of the undoped two-orbital Hamiltonian was carried out. NN and NNN Heisenberg interactions $J_{\rm NN}$ and $J_{\rm NNN}$ were obtained. This strong coupling expansion for multiorbital models is subtle and it has to be performed in such a way that the results are independent of the basis chosen for the orbitals. Following, e.g., [17] these additional interactions are $\sum_{\langle \mathbf{ij} \rangle, \alpha\beta} J_{ij} \mathbf{S}_{\mathbf{i}\alpha} \cdot \mathbf{S}_{\mathbf{j}\beta}$, , where $\langle \mathbf{ij} \rangle$ indicates NN and NNN sites with $J_{ij} = J_{\rm NN}$ and $J_{\rm NNN}$, $\{\alpha, \beta\}$ label the orbitals (x or y), and $\mathbf{S}_{\mathbf{i}\alpha}$ is the total spin at site $\mathbf{i}$ and orbital α. The couplings are $J_{\rm NN} = \frac{2(t_1^2+t_2^2)}{3(U+J_H)}$ and $J_{\rm NNN} = \frac{4(t_3^2+t_4^2)}{3(U+J_H)}$, where t_i are the hoppings $t_1 = -1$, $t_2 = 1.3$, $t_3 = t_4 = -0.85$ in the usual notation [12] ($|t_1|$ units). $J_{\rm NN}$ and $J_{\rm NNN}$ are the same for both orbitals. The ratio $\frac{J_{\rm NN}}{J_{\rm NNN}} = \frac{1}{2}\frac{t_1^2+t_2^2}{t_3^2+t_4^2} = 0.93$ is kept fixed since $J_{\rm NN}$ and $J_{\rm NNN}$ are both antiferromagnetic, and a ratio ~1 introduces frustration favoring $(\pi, 0)$-$(0, \pi)$ spin order, as confirmed by calculating the spin structure factor and varying $J_{\rm NN}/U$ [18]. Below, $J_{\rm NN}$ will be considered a free parameter independent of U and J_H (with $J_{\rm NN}/J_{\rm NNN} = 0.93$), to further enhance such a spin order.

By adding the extra Heisenberg terms to the two-orbital model, the desired goal is obtained since with increasing $J_{\rm NN}$ eventually E_B becomes negative for all the studied (U, J_H) couplings. The spin-triplet region virtually disappears [Fig. 1(b)] and it is mainly replaced by the B_{2g} state which itself becomes confined to $U < 4|t_1|$ (squares) due to the expansion of the A_{1g} region. The symmetries shown in Fig. 1(b) were obtained with the smallest superexchange values $(J^*_{\rm NN}, J^*_{\rm NNN})$ that produce binding of two electrons at each (U, J_H) point. In Fig. 2(a), where the binding energy versus $J_{\rm NN}/U$ is shown at several U's and at a fixed (realistic) $J_H/U = 0.2$, some examples of $(J^*_{\rm NN}, J^*_{\rm NNN})$ can be found. Increasing $J_{\rm NN}$ eventually induces binding for all U's. The value of $J_{\rm NN}/U$ for which binding occurs decreases as U increases.

Studying E_B and the relative symmetry between the $N = 16$ and 18 GSs, phase diagrams in the $(U, J_{\rm NN}/U)$ plane were constructed. In Fig. 2(b), typical results for $J_H/U = 0.2$ are shown [19]. The bound state has A_{1g} symmetry in most of the binding region, but a B_{2g} symmetric state also prevails at small U values ($\sim 2|t_1|$). Both symmetries appear inside the proper magnetic or metallic region of the undoped limit, according to mean-field calculations [20] extended to incorporate $J_{\rm NN}$. In [18] it is

shown that the results in Figs. 2(a) and 2(b) are qualitatively the same varying J_{NN}/J_{NNN} in the range [0.5, 1.5].

Overlaps.—Consider now the pairing operators that produce the electronic bound states. The overlap $\langle\Psi(N=18)|\Delta^\dagger_{\mathbf{k},i}|\Psi(N=16)\rangle$ was calculated, where $|\Psi(N)\rangle$ is the GS in the subspace of N electrons and $\Delta^\dagger_{\mathbf{k},i} = \sum_{\alpha\beta} f(\mathbf{k})(\sigma_i)_{\alpha\beta} d^\dagger_{\mathbf{k},\alpha,\uparrow} d^\dagger_{\mathbf{k},\beta,\downarrow}$, with $d^\dagger_{\mathbf{k},\alpha,\sigma}$ creating an electron with spin z-axis projection σ, at orbital $\alpha = x, y$, and with momentum $\mathbf{k}$. The structure factor $f(\mathbf{k})$ arises from the spatial location of the electrons forming the pair [6], and σ_i are the Pauli matrices ($i = 1, 2, 3$) or the 2×2 identity matrix σ_0 ($i = 0$) (note that σ_1 and σ_2 imply an interorbital pairing). Overlaps for all the symmetries in [6], and with NN and NNN locations for the electronic pairs, were evaluated.

For all operators respecting the relative symmetry between the doped and undoped states, finite overlaps were found, although of different values. As a trend, as the binding grows, pairing involving NNN operators prevail over the NN ones. For example, in the A_{1g} region in Fig. 2(b) there are four pairing operators with finite overlap [shown in Fig. 3(a) for $U = 3|t_1|$ and $J_H/U = 0.2$] characterized by $f(\mathbf{k})\sigma_i$ equal to (i) $(\cos k_x + \cos k_y)\sigma_0$ (full circles), (ii) $(\cos k_x \cos k_y)\sigma_0$ (full squares), (iii) $(\sin k_x \sin k_y)\sigma_1$ (full diamonds), and (iv) $(\cos k_x - \cos k_y)\sigma_3$ (full triangles). Close to the boundary with the B_{2g} phase where the binding is weak ($E_B \approx -0.05|t_1|$), operators (i) and (ii) present the largest, and almost equal, overlaps. With increasing binding the (i) overlap decreases while (ii) becomes stronger. The overlaps for operators (iii) and (iv) are clearly smaller.

Note that (ii) is the simplest expression of a nodeless $s\pm$ pairing operator [21]. Our results indicate that this type of pairing dominates only when the binding energy is large, which occurs at very large U or J_{NN}. At intermediate values of couplings, a *symmetric* linear combination of (i) and (ii) with almost equal weights is optimal, and it leads to a "quasinodal" $s\pm$ pairing state [Fig. 3(b)]. From this perspective, the most "natural" A_{1g} pairing operator arises from a linear combination of (i) and (ii), as opposed to just (ii) as in $s\pm$ scenarios. The gaps in Fig. 3(b) were calculated from mean-field approximations as in [6,22] and choosing a pairing strength V_0 such that the gap order-of-magnitude in meV agrees with experiments [16]. Note that the linear combination A_{1g^+} for the hole pockets closely reproduces (full and dashed lines) the ARPES results in the superconducting state, with both gaps only weakly $\mathbf{k}$ dependent, and with the interior (exterior) pocket gap ~12 (6) meV. The electron pockets, on the other hand, present strongly $\mathbf{k}$-dependent gaps, and a quasinode is found along the x (y) axes for the pocket at X (Y). In the folded zone, this implies that the quasinode is on the outer pocket, in agreement with angle-resolved specific heat measurements [23].

Note that the presence of a d_{xy} "patch" on the electron pockets has been discussed before by many groups as possibly responsible for gap nodes (or minima) on the electron pockets. The present results show that such a minimum (or nodes) can arise *without* such an xy patch, which is important to assess the impact of the various orbitals. The one-particle spectral function $A(\mathbf{k}, \omega)$ was also calculated [18]. Features on the scale of the magnetic or superconducting gaps cannot be resolved within the few momenta available, but the higher energy features at intermediate couplings are

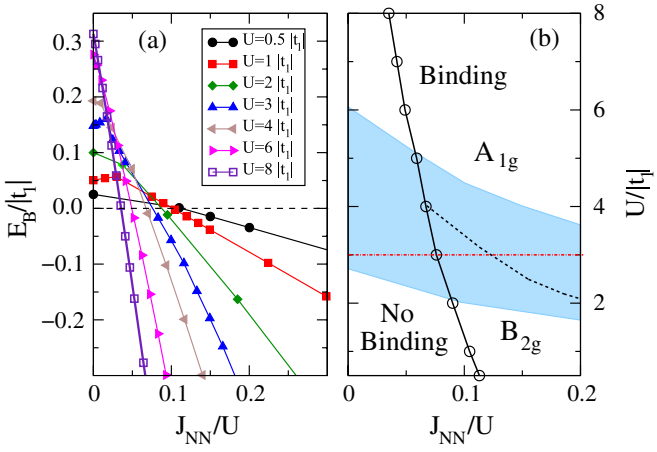

FIG. 2 (color online). (a) $E_B/|t_1|$ versus J_{NN}/U for different values of $U/|t_1|$ and $J_H/U = 0.2$. (b) Phase diagram showing "Binding" and "No Binding" regions and the symmetry of the two-electron bound state varying $U/|t_1|$ and J_{NN}/U, for $J_H/U = 0.2$. The shaded area is where the antiferromagnetic or metallic state is stabilized in the mean-field approximation for the undoped limit. The dot-dashed line is for Fig. 3.

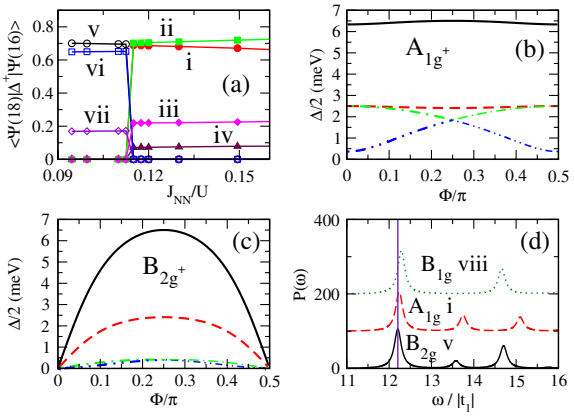

FIG. 3 (color online). (a) Overlap $\langle\Psi(N=18)|\Delta^\dagger_{\mathbf{k},i}|\Psi(N=16)\rangle$ versus J_{NN}/U for the indicated pairing operators, at $U = 3|t_1|$ and $J_H/U = 0.2$. (b) Superconducting gap at the FS: internal hole pocket (continuous line), external hole pocket (dashed line). The dot-dashed and double dot-dashed lines are for the two-electron pockets which intersect at the Brillouin zone boundary ($\Phi = \pi/4$) of the folded zone. The A_{1g^+} symmetric linear combination of A_{1g} operators (i) and (ii) is used, with equal weight. The angle Φ is measured from the positive x axis to the positive y axis. (c) Same as (b) but for the B_{2g^+} symmetric combination of the B_{2g} operators (v) and (vi). (d) Dynamic pairing susceptibility for the pairing operators indicated (see text), at $U = 3|t_1|$, $J_H/U = 0.2$, and $J_{NN}/U = 0.095$. The vertical line indicates $E(18) - E(16)$.

similar to noninteracting bands [20], in agreement with ARPES experiments and with local density approximation plus dynamical mean-field theory calculations [24].

As mentioned before, in physically relevant portions of the phase diagram [20] the pairing symmetry B_{2g} competes with A_{1g}. Three B_{2g} pairing operators with finite overlaps were found in this region: (v) $(\cos k_x + \cos k_y)\sigma_1$, (vi) $(\cos k_x \cos k_y)\sigma_1$, and (vii) $(\sin k_x \sin k_y)\sigma_0$. From Fig. 3(a) the interorbital operators (v) and (vi) have a much larger GS overlap than the intraorbital operator (vii). The mean-field calculation of the gaps for the symmetric combination of the prevailing B_{2g} pairing operators, i.e., (v) + (vi), is in Fig. 3(c). All the gaps have nodes along the x and y axes, also in good agreement with [23]. A strong $\mathbf{k}$ dependence is observed for all FS pockets, and the electron-pocket gaps are small (~ 1 meV).

Dynamical pair susceptibilities.—To complete our analysis the dynamical pair susceptibilities, defined by $P(\omega) = \int_{-\infty}^{\infty} dt e^{i\omega t} \langle \Delta_{\mathbf{k},i}(t) \Delta_{\mathbf{k},i}^{\dagger}(0) \rangle$, were also studied in the state with $N = 16$ for the pairing operators $\Delta_{\mathbf{k},i}$. A procedure used in the context of the cuprates will be followed [25]. Results for $U = 3|t_1|$, $J_H/U = 0.2$, and several values of J_{NN}/U were obtained along the dot-dashed (red) line of Fig. 2(b). The overlaps calculation already indicated that for $N = 18$ there are several low-lying energy states with different symmetries near the GS. The dynamical pair susceptibilities show that most of these low-lying states have a large overlap with $\Delta_{\mathbf{k},i}^{\dagger}|\Psi_{N=16}(0)\rangle$ for $\Delta_{\mathbf{k},i}^{\dagger}$ with the appropriate symmetry. This is *qualitatively different* from the cuprates' t-J model, where the overlap of the doped GS with $\Delta_{\mathbf{k},i}^{\dagger}|\Psi(0)\rangle$ was large for Δ with d-wave symmetry but negligible for s-wave symmetry [25]. In that s-wave case the spectral weight in $P(\omega)$ accumulates at high energies, while $P(\omega)$ for the d-wave pairing operator showed a well-defined sharp peak at the GS energy of the doped state [25]. This is not the case for the two-orbital model. For example, in Fig. 3(d) at $J_{\mathrm{NN}}/U = 0.095$, where the doped GS has symmetry B_{2g}, a sharp peak occurs in $P(\omega)$ for the B_{2g} pairing operator (v), but a similar behavior is found in $P(\omega)$ for the A_{1g} pairing operator (i) (the low-lying peak originates in a low-lying excited state with A_{1g} symmetry). In addition, the susceptibility for a pairing operator (viii) $(\cos k_x + \cos k_y)\sigma_3$, NN version of the B_{1g} operator (ix) $(\cos k_x \cos k_y)\sigma_3$, is also competitive [26] [Fig. 3(d)].

Conclusions.—The effects of NN and NNN Heisenberg terms on the symmetry and the binding energy of two electrons added to the undoped state of the two-orbital Hubbard model were studied using Lanczos techniques on small clusters. Quasinodal A_{1g} bound states are stabilized for physical values of J_H/U, in the intermediate or large U region, in agreement with RPA results [4]. Our results also indicate that a competing B_{2g} state may become stable in physically relevant regimes of $U/|t_1|$. In addition, the pairing susceptibility presents low-lying excitations with B_{2g}, A_{1g}, and B_{1g} symmetries. Thus, pairing correlations with any of these symmetries could be stabilized by small modifications in the model parameters, in agreement with [4–6,10]. This suggests that a similar sensitivity to small details may occur among different compounds of the pnictide family.

This work was supported by the U.S. DOE, Office of Basic Energy Sciences, Materials Sciences and Engineering Division (A. N., W. G., X. Z., G. M., A. M., E. D.), CONICET, Argentina (J. R.), the DFG under the Emmy-Noether program (M. D.), and by the Foundation for Polish Science (FNP) and the Polish government Project N202 069639 (A. M. O.). Conversations with D.-X. Yao and Thomas Prestel are acknowledged.

[1] D. C. Johnston, Adv. Phys. **59**, 803 (2010).
[2] See, for instance, T. Kondo *et al.*, Phys. Rev. Lett. **101**, 147003 (2008); H. Ding *et al.*, Europhys. Lett. **83**, 47 001 (2008).
[3] H.-J. Grafe *et al.*, Phys. Rev. Lett. **101**, 047003 (2008); J. K. Dong *et al.*, Phys. Rev. Lett. **104**, 087005 (2010).
[4] S. Graser *et al.*, New J. Phys. **11**, 025016 (2009).
[5] M. Daghofer *et al.*, Phys. Rev. Lett. **101**, 237004 (2008).
[6] A. Moreo *et al.*, Phys. Rev. B **79**, 134502 (2009).
[7] E. Dagotto *et al.*, Phys. Rev. B **45**, 10 741 (1992).
[8] C. de la Cruz *et al.*, Nature (London) **453**, 899 (2008).
[9] E. Dagotto, Rev. Mod. Phys. **66**, 763 (1994).
[10] Q. Si and E. Abrahams, Phys. Rev. Lett. **101**, 076401 (2008); K. Seo, B. A. Bernevig, and J. Hu, Phys. Rev. Lett. **101**, 206404 (2008).
[11] L. Arrachea and D. Zanchi, Phys. Rev. B **71**, 064519 (2005), and references therein.
[12] S. Raghu *et al.*, Phys. Rev. B **77**, 220503 (2008).
[13] L. Boeri, O. V. Dolgov, and A. A. Golubov, Phys. Rev. Lett. **101**, 026403 (2008).
[14] A. M. Oleś, Phys. Rev. B **28**, 327 (1983).
[15] A similar symmetry analysis can be used to improve cluster dynamical mean-field theory calculations; see E. Koch, G. Sangiovanni, and O. Gunnarsson, Phys. Rev. B **78**, 115102 (2008).
[16] From comparisons with [13] we set $|t_1| = 0.2$ eV.
[17] A. M. Oleś *et al.*, Phys. Rev. B **72**, 214431 (2005).
[18] See supplemental material at http://link.aps.org/supplemental/10.1103/PhysRevLett.106.217002 for results.
[19] For $J_H/U = 0.3$ (0.1) the phase diagram Fig. 2(b) was found to be qualitatively similar to the $J_H/U = 0.2$.
[20] R. Yu *et al.*, Phys. Rev. B **79**, 104510 (2009); Q. Luo *et al.*, Phys. Rev. B **82**, 104508 (2010).
[21] I. Mazin *et al.*, Phys. Rev. Lett. **101**, 057003 (2008); K. Kuroki *et al.*, Phys. Rev. Lett. **101**, 087004 (2008).
[22] M. Daghofer *et al.*, Phys. Rev. B **81**, 014511 (2010).
[23] B. Zeng *et al.*, Nature Commun. **1**, 112 (2010).
[24] M. Aichhorn *et al.*, Phys. Rev. B **80**, 085101 (2009); P. Hansmann *et al.*, Phys. Rev. Lett. **104**, 197002 (2010).
[25] E. Dagotto, J. Riera, and A. P. Young, Phys. Rev. B **42**, 2347 (1990).
[26] $P(\omega)$'s for $J_{\mathrm{NN}}/U = 0.20$, inside the A_{1g} pairing region, were also studied. No qualitative changes were found.